Journal of Solid State Electrochemistry (2020) 24:1271–1282
https://doi.org/10.1007/s10008-020-04615-0

ORIGINAL PAPER

Improved electrochemical performance of supercapacitors by utilizing ternary Pd-AC-doped NiO nanostructure as an electrode material

Sonal Singhal[1] · A.K. Shukla[1]

Received: 12 February 2020 / Revised: 31 March 2020 / Accepted: 22 April 2020 / Published online: 9 May 2020

Abstract

Recent applications of supercapacitors in modern society are limited due to their poor electrochemical properties like energy density and cyclic stability, etc. One of the effective approaches to boost the electrochemical performance is to couple the metal oxide with metal and carbon nanostructures. In this study, hybrid ternary nanocomposite, comprised of palladium, activated carbon, and nickel oxide nanoparticles (Pd-AC@NiO), has been synthesized through a simple approach. Here, metal-carbon material plays a significant role in augmenting the specific surface area, while the existence of NiO nanoparticles provides the electroactive sites for energy storage. Consequently, the as-prepared Pd-AC@NiO nanocomposite provides excellent electrochemical performance compared to the as-prepared NiO nanoparticles as an electroactive material. When the hybrid ternary nanocomposite is used as an electroactive material for supercapacitor, it displays an outstanding specific capacitance of 1539 F/g at a current density of 5 A/g in a three-electrode system. Moreover, in terms of energy and power, the as-prepared hybrid ternary nanocomposite electrode demonstrates a high energy density of 34.19 Wh/kg and power density of 1000 W/kg. Additionally, the resulting hybrid ternary nanocomposite electrode shows excellent cycling stability with the capacity retention of 95.5% after 5000 cycles. Thus, these outcomes suggest that the proposed composite material has tremendous electrochemical properties. It deliberated as a promising electrode for the development of energy storage devices with high energy and power densities.

Keywords Supercapacitors · Pd-activated carbon · NiO nanoparticles · Electrochemical performance · Energy storage

Introduction

Nowadays, energy storage systems have attracted much attention in electronic devices and electric vehicles, etc. Among the energy storage devices, batteries and fuel cells have been considerably scrutinized [1–4]. Batteries and fuel cells are extensively renowned as a tempting device to harvest the stored energy via chemical processes. Compared to batteries and fuel cells, supercapacitors are used to store energy via charge separation at the interface of electrolyte ions and electrodes. Supercapacitors have enticed enormous attention due to some superior merits such as high power density than batteries, long cycle life, and higher energy density than conventional dielectric capacitors [5–7]. All the aforementioned intriguing features make supercapacitors a promising energy storage device and also create a great interest in a wide range of applications, such as hybrid electric vehicles, industrial power management, memory backup systems, and consumer electronics [8–10]. Due to their substantially high power density and reasonable energy density, supercapacitors can act as a bridge between batteries and conventional dielectric capacitors. However, many challenges still exist that need to be addressed for the practical application of supercapacitors as emerging technologies into the market. One of the major hurdles of the supercapacitors is to increase energy efficiency without sacrificing power density and cycle life because high power density and long cycle life are also desirable for practical applications. Therefore, the improvement in the energy density of supercapacitors can achieve by maximizing the specific

Electronic supplementary material The online version of this article (https://doi.org/10.1007/s10008-020-04615-0) contains supplementary material, which is available to authorized users.

✉ A.K. Shukla
akshukla@physics.iitd.ernet.in

[1] Laser-Assisted Materials Processing and Raman Spectroscopy Laboratory, Department of Physics, Indian Institute of Technology Delhi, New Delhi 110016, India

capacitance. To enhance the specific capacitance and to fulfill the demand of high-performance energy storage devices in terms of high power and energy densities for practical applications, high specific surface area, optimum pore size distribution, and wettability behavior of the electrode materials play an important role in ensuring the excellent performance of supercapacitors [11–14].

Till to date, various metal oxide-based materials, such as MnO_2, TiO_2, V_2O_5, CuO, and NiO, have been explored as electrode materials for supercapacitors aimed at high specific capacitance, high energy density, high power density, and good cycling stability [15–20].Among them, NiO is a promising material due to its environmentally friendly nature, high theoretical capacitance, low cost, and a wide range of preparation strategies [18–20]. However, the low electrical conductivity, poor long-term stability, and poor rate performance restrict their practical applications. In order to enhance the supercapacitor performance of NiO, several efforts have been made by metal coating or doping and incorporating with carbon materials. Yuan et al. prepared Cu-doped NiO material by the citrate gel process and reported a capacitance of 559 F/g at 0.3 A/g [21]. Nagamuthu et al. reported Ag/NiO honeycomb nanoarrays as an electrode material with enhanced electrochemical performance for supercapacitors [22]. This Ag/NiO honeycomb nanoarrays electrode delivered a maximum specific capacity of 824 C/g at a specific current of 2.5 A/g. Al-doped NiO nanosheet array for supercapacitor application was reported by Chen et al. [23]. In this study, the Al-doped NiO nanosheet array was fabricated by hydrothermal reaction and heat treatment. They found Al-doped NiO nanosheet array delivers a high specific capacitance of 2253 F/g at a current density of 1 A/g with good cyclic stability.Wang et al. reported NiO/Ag nanocomposite synthesized from the micro-emulsion method [24]. NiO/Ag nanocomposite yielded 322 F/g specific capacitance at a current density of 1 A/g. Vijayakumar et al. used a porous NiO/C nanocomposite as electrode material for supercapacitor application and reported a specific capacitance of 644 F/g at a scan rate of 2 mV/s [25].Chen et al. reported NiO/graphene aerogel nanocomposite as a supercapacitor electrode material with a tiny decay in cycling stability after 1000 cycles [26]. Meanwhile, it is renowned that an ideal electrode material for high-performance supercapacitor should possess a high electrical conductivity and large specific surface area. Literature survey shows that among various materials, some noble metals like silver, gold, platinum, ruthenium, and palladium with metal oxides, carbon materials and conducting polymers have fascinated much consideration in the field of electrode materials of supercapacitors due to their good electrical conductivity and electrochemical stability [27–30]. Due to their high electrical conductivity, noble metals can facilitate effective transport of electrons during charge-discharge cycles. However, due to the paucity and high cost of noble metals, their amalgamation with other sustainable and cheap materials is considered one of the most attractive ways to optimize their properties and minimize their consumption. Hence, it is essential to develop a supercapacitor electrode material by combining a noble metal with other cost-effective materials that can improve the electrochemical performance of the supercapacitors. In order to meet this challenge, several carbon nanostructures, such as carbon nanotubes (CNTs), activated carbon (AC), and carbon nanospheres (CNSs) have been validated for achieving better electrochemical performance [31–34] because it can improve the electrical conductivity and specific surface area. It also provides more numbers of accessible active sites for reactions, which benefits to rate capability and cycling ability. With this consideration, to see the effect of different properties of metal, metal oxides and carbon materials in the capacitive performance, hybrid ternary composite electrodes have fabricated by combining metal nanostructures and metal oxides with carbon materials [24, 31–35]. Until now, there are only few reports based on the use of palladium noble metal for supercapacitor application [30, 36, 37]. Therefore, the use of Pd for supercapacitor application is still a big challenge. In the present article, we carefully used palladium noble metal because it can provide high surface area for adsorption of ions, which leads to high specific capacitance. Therefore, overall better electrochemical performance can be achieved due to the combined properties of carbon, metal, and metal oxide. With this aim, in the current study, we report the fabrication of hybrid ternary nanocomposite (Pd-AC@NiO) by combining palladium (Pd), activated carbon (AC), and nickel oxide nanoparticles (NiO) and further used as an electrode material for supercapacitors application. Activated carbon owns several advantages, which makes them suitable for utilizing as an electrode material for supercapacitor. They possess large specific surface area and moderate electrical conductivity, which makes activated carbon a suitable support for enhancing the specific surface area and electrical conductivity of metal oxides when utilized as an electrode material for supercapacitors. Palladium (Pd) enhances the electrical conductivity of the NiO nanoparticles, which is more favorable for the energy storage devices. Therefore, the combination of Pd-activated carbon (Pd-AC) and NiO may greatly enhance the capacitive performance of the electrode for supercapacitor applications due to the large specific surface area and high wettability by an aqueous electrolyte.Their electrochemical characteristics have demonstrated that the specific capacitance of the Pd-AC@NiOnanocomposite electrode is superior (1539 F/g) in comparison with that of the NiO-based electrode (1190 F/g). Furthermore, the as-prepared hybrid ternary composite electrode demonstrates a high energy and power densities (energy density of 34.19 Wh/kg at a power density of 1000 W/kg). Moreover, the resulting hybrid ternary composite electrode shows remarkably excellent cycling stability with the capacity retention of 95.5% after 5000 cycles.

Experimental section

Materials

All reagents purchased were of analytical grade (AR) and commercially available. Nickel chloride and polyvinylidene fluoride (PVDF) were procured from Alfa Aesar. Polyvinyl alcohol (PVA), potassium hydroxide (KOH), ethanol, and N-methyl-2-pyrrolidone (NMP) were acquired from Fisher Scientific Pvt. Ltd. Activated carbon was purchased from MERCK. Palladium nitrate dihydrate ($Pd(NO_3)_2$. $2H_2O$) was purchased from Central Drug House P. Ltd., India. All chemicals were used as received without any purification.

Synthesis of NiO nanoparticles

Nickel oxide nanoparticles (NiO NPs) were prepared by the co-precipitation method using nickel chloride and PVA as starting materials and de-ionized water as dispersing solvent. The synthesis procedure was described as follows: 4 g of nickel chloride was dissolved in 100 mL of de-ionized water. The obtained solution was magnetically stirred for 2 h. PVA solution was prepared by the dissolution of PVA into de-ionized water under stirring. Then, the PVA solution was added drop-wise to the nickel chloride solution to prevent particle aggregation. Here, PVA acts as a stabilizer, which prevents particle aggregation that facilitates the formation of uniform nanoparticles. Afterward, the resultant solution was stirred for 4 h at 60°C. The precipitate was collected and then dried at 100°C for 2 h. Finally, the obtained material was ground well with a pestle and mortar and then annealed in a furnace at a ramping rate of 3°C/min with a temperature of 700°C for 2 h under inert ambiance. After cooling down to room temperature, the sample was taken out for further use.

Synthesis of Pd-AC@NiO nanocomposite

A typical synthesis procedure for Pd-AC@NiO nanocomposite was described as follows: 0.5 g of prepared NiO NPs were added into 20 mL of ethanol and was sonicated for 60 min until the nanoparticles were dissolved completely. Then, a mixed solution was prepared by dissolving 0.4 g palladium nitrate dihydrate ($Pd(NO_3)_2$. $2H_2O$) and 0.35 g activated carbon (AC) in the 40 mL of ethanol and was then sonicated for 30 min. The solution containing metal salt and AC was then transferred to the prepared NiO NPs solution under magnetic stirring until a homogeneous solution was obtained. Then, the NaOH solution was added to the above solution to adjust the pH value, which is important for nanoparticle formation. The reaction solution was kept at 90°C for 2 h under magnetic stirring. After the reaction, the product was collected by filtration. Subsequently, the product was washed with ethanol and DI water. Then, the as-synthesized Pd-AC@NiO nanocomposite was thermally decomposed at 600°C for 2 h under an Ar atmosphere with a ramping rate of 3°C/min in a tube furnace.

Characterization

The crystallographic structures were determined by X-ray diffraction (XRD) using a Rigaku Ultima- IV X-ray diffractometer equipped with Cu Kα radiation ($\lambda = 1.54$ Å). Transmission electron microscopy was performed using a Tecnai G2 20 system with 200 kV for investigating the microstructure of the samples. The morphology of the sample was investigated by field emission electron microscopy (FESEM) using a JEOL JSM-7800F Prime. X-ray photoelectron spectroscopy (XPS) was executed on a PHI VersaProbe III spectrometer using a monochromatized Al Kα radiation (1486.6 eV). The XPSPEAK software accomplished the deconvolution of the XPS peak. Compositional studies and elemental mapping of the samples were carried out by energy-dispersive X-ray spectroscopy (EDX) using QuanTax 200 spectrometer. N_2 adsorption and desorption isotherms were conducted on a Quantachrome Nova Station Version 3 at 77 K. Before adsorption, the samples were degassed at 200 °C for 6 h. The Brunauer-Emmett-Teller (BET) adsorption method calculated the specific surface area and the Barret-Joyner-Halenda (BJH) method estimated the pore size distribution of all the samples. The contact angle measurements were done on a KRUSS ADVANCE system. The contact angle value was the average of five measurements at different positions using a sessile drop method.

Fabrication of electrode for electrochemical characterization

All the electrochemical measurements were performed in a standard three-electrode system. In the three-electrode system, the fabricated electrode using NiO NPs and Pd-AC@NiO nanocomposite, platinum wire, and standard calomel electrode (SCE) was used as the working electrode, counter electrode, and reference electrode respectively. In detail, the working electrode was prepared by mixing the active materials (NiO NPs, Pd-AC@NiO), and PVDF in N-methyl-2-pyrrolidone (NMP) solvent with a mass ratio of 90:10. After mixing, the slurry was directly pasted onto a copper foil, and then the fabricated electrodes were dried at 90°C for 2 h. The weight of the active materials was kept the same while preparing the electrodes using NiO NPs and Pd-AC@NiO nanocomposite. The electrochemical performance of the prepared electrode was accomplished by cyclic voltammetry (CV), galvanostatic charging-discharging measurements (GCD), and cyclic stability. All of the above electrochemical performances were conducted using a CHI electrochemical workstation. CV measurements were carried out at various scan rates within the

potential difference ranging from −1.8 V to 0.2 V. Galvanostatic charging-discharging assessments were conducted in the potential range of 0 to 0.4 V at various current densities. The cyclic stability test was carried out within the potential difference ranging from 0 to 0.4 V at a constant current density for 5000 charging-discharging cycles. All the electrochemical tests were executed at room temperature with a 2 M KOH aqueous solution as the electrolyte. The specific capacitance of the prepared electrode derived from CV curves and galvanostatic charging-discharging curves by three-electrode testing were, respectively, calculated via equation

$$CS = \frac{\int I\, dV}{m\, v\, \Delta V}$$

and

$$CS = \frac{I\, \Delta t}{m\, \Delta V}$$

where C_S is the specific capacitance (F/g), and I is the current (A). The integral term is the area under the CV curve, m is the mass of the active material (g), v is the scan rate (V/s), Δt is the discharge time (s), and ΔV is the working potential window (V).

To evaluate the energy storage performance of the prepared electrodes, energy density and power density were two important parameters. Meanwhile, the energy density and power density in terms of mass were evaluated using a galvanostatic charging-discharging test by the following Eqs. $E = \frac{C_S(\Delta V)^2}{2}$ x $\frac{1}{3.6}$ and.

$P = \frac{E}{\Delta t} \times 3600$, respectively, where E is the energy density (W h/Kg), and P is the power density (W/Kg).

Results and discussion

Morphological, structural, and wettability analysis of the NiO nanoparticles and Pd-AC@NiOnanocomposite

Morphology and structure of the as-prepared samples are explored using field emission scanning electron microscopy (FESEM) and transmission electron microscopy (TEM). Fig. 1a and S1 illustrate the FESEM images of the as-prepared NiO and Pd-AC@NiO nanocomposite, respectively. It is observed in Fig. S1 that the prepared NiO sample is composed of small particles.

The shape of the NiO nanoparticles does not change after incorporating Pd-AC into NiO while a slight change in particle size is detected shown in Fig. 1a. TEM images of the as-prepared Pd-AC@NiO nanocomposite (Fig. 1b) show that the particles are well distributed and have a diameter range from 20 nm to 120 nm. Particle size for the obtained Pd-AC@NiO nanocomposite is measured from the TEM images, and the particle size distribution profile is plotted in Fig. 1c. In particular, Pd-AC@NiO nanocomposite shows an average particle size of 80 nm. To have a clear observation of the chemical composition of the prepared nanocomposite (Pd-AC@NiO), energy-dispersive X-ray spectroscopy (EDS) analysis, and elemental mapping analysis have been studied. The elemental spectra (Fig. 2a) and mapping results (Fig. 2b-f) of the Pd-AC@NiO nanocomposite confirm the presence of palladium (Pd), nickel (Ni), carbon (C), oxygen (O), and platinum (Pt) components in the Pd-AC@NiO. It is found that the Pd-AC@NiO nanocomposite contains a platinum element, as shown in Fig. 2a, because it is used as a coating material in preparing a sample for EDX analysis. Therefore, the existence of the Pt element in the prepared nanocomposite is likely from the sputter coating during the sample preparation for EDS analysis. For comparison, elemental analysis of pure synthesized NiO is also investigated, and results are displayed in the supplementary information (Fig. S2). The results demonstrate that the synthesized NiO is composed of its four components, namely, nickel (Ni), oxygen (O), carbon (C), and platinum (Pt). The observed nickel and oxygen peaks are due to the composition of the catalyst, while the Pt signal arises from the sputter coating during the sample preparation, and the C signal is due to the carbon tape on which the material has adhered for EDS analysis. Elemental mapping results (Fig. 2b-f) confirm that the Pd-AC composite has been successfully incorporated into the NiO nanostructure.

Besides, X-ray photoelectron spectroscopy (XPS) is carried out to further investigate the chemical properties and surface elemental composition of synthesized Pd-AC@NiO nanocomposite, and the results are shown in Fig. 3. The high-resolution Pd 3*d* core-level XPS spectrum of Pd-AC@NiO nanocomposite is shown in Fig. 3a. As displayed in Fig. 3a, the deconvolution of the Pd 3*d* spectrum discloses the presence of a doublet that consists of a high-energy band at 339.39 eV and a low energy band at 334.59 eV correspond to the Pd3$d_{5/2}$ and Pd 3$d_{3/2}$, which are in accordance with the reported values for Pd° species [38]. Therefore, the high-resolution Pd 3*d* spectrum reveals that the attached Pd on to the surface of nanocomposite exists in the form of Pd°. The high-resolution C 1*s* spectrum of Pd-AC@NiO in Fig. 3b can be deconvoluted into two peaks. One peak at the binding energy of 284.9 eV is ascribed to the C-C bond, and the other peak at the binding energy of 285.9 eV corresponds to the C-O bond, indicating the existence of oxygen-containing functional groups [39]. The oxygen-containing functional groups can be identified from the O 1*s* spectrum of Pd-AC@NiO in Fig. 3c. The O 1 *s* spectrum in Fig. 3c displays two peaks at 531 eV and 533.3 eV, corresponding to the binding energies of O 1 *s* in Ni-O-H and O-C, respectively, which can enhance the wettability [40].

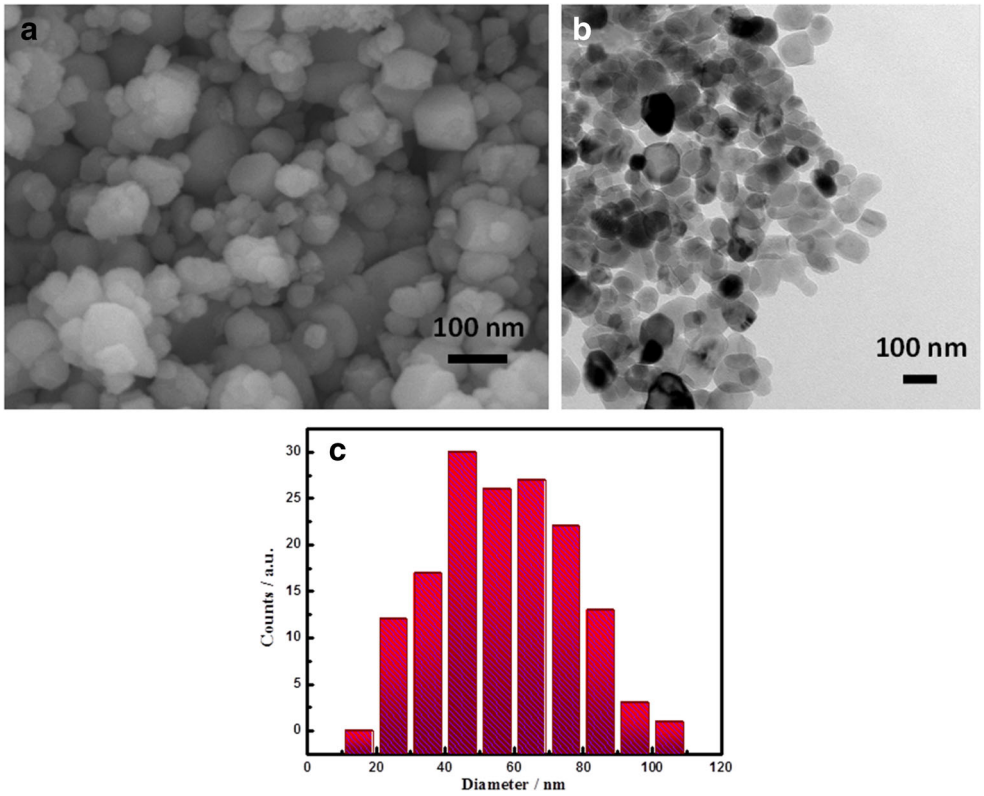

Fig. 1 **a** FESEM image of Pd-AC@NiO nanocomposite. **b** TEM image of Pd-AC@NiO nanocomposite. **c** Particle size distribution for Pd-AC@NiO nanocomposite determined from TEM images

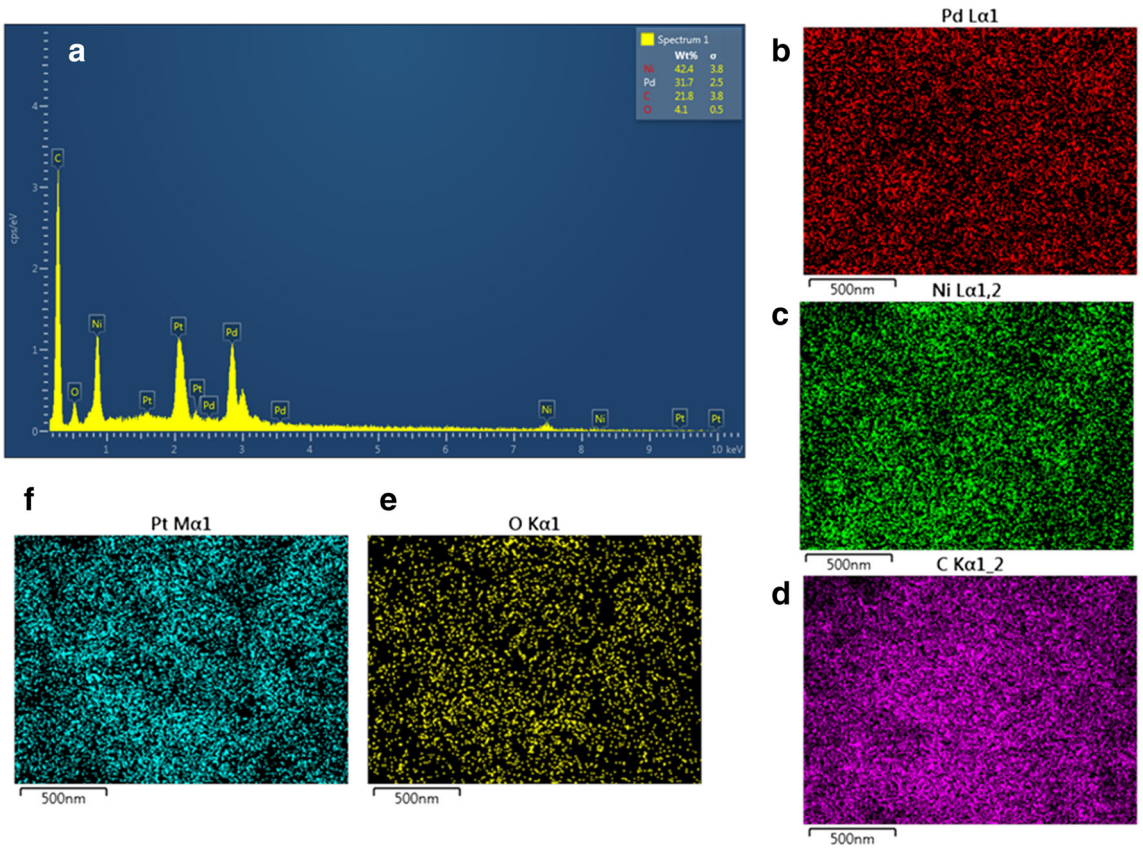

Fig. 2 **a** Elemental spectra of Pd-AC@NiO nanocomposite. **b-f** Elemental mapping images of palladium, nickel, carbon, oxygen, and platinum of Pd-AC@NiO nanocomposite

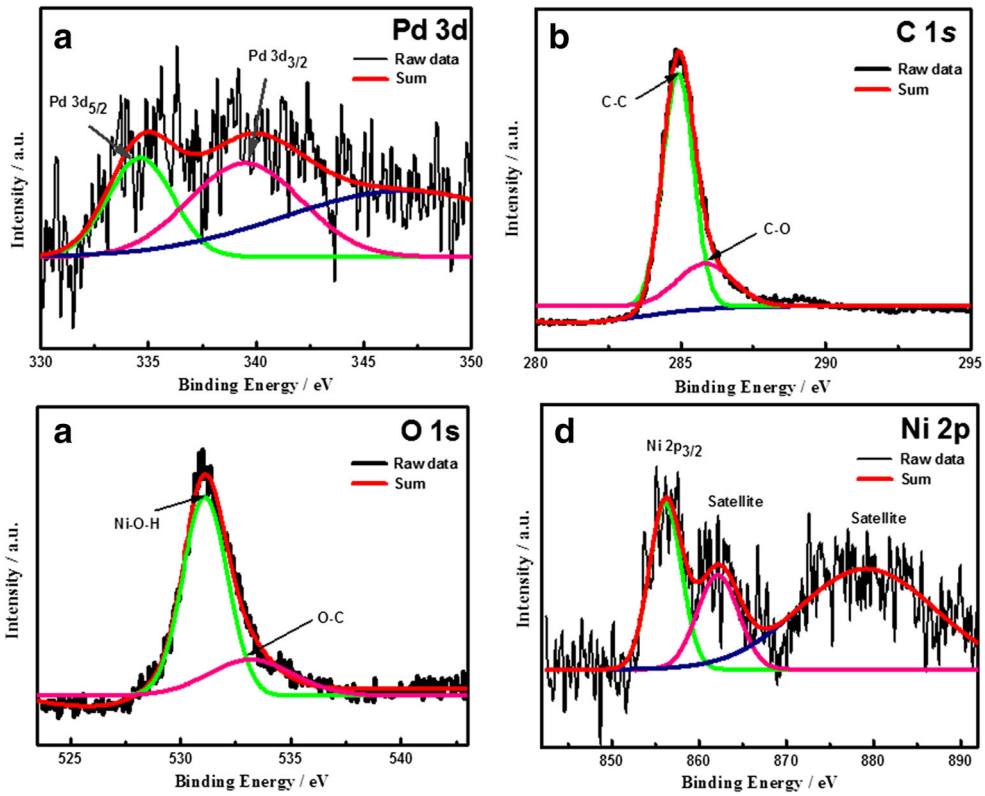

Fig. 3 High resolution XPS spectra (**a**) Pd 3*d*, (**b**) C 1 *s*, (**c**) O 1 *s*, and (**d**) Ni 2*p* for Pd-AC@NiO nanocomposite

Wettability is an important parameter for enhancing the electrochemical performance of the electrode material, which can easily improve the access of the electrolytic ions into the electrode surface. Therefore, a contact angle measurement is performed to determine the nature of the electrode surface and is displayed in Fig. S3. The contact angle of the Pd-AC@NiO based electrode is 52.7°. It indicates that the surface is hydrophilic, which can improve the electrochemical performance. Fig. 3d shows the Ni 2*p* spectrum of Pd-AC@NiO. The Ni 2*p* spectrum in Fig. 3d displays a complex structure along with two strong satellite signals and one main peak due to the multi-electron excitation. Ni $2p_{3/2}$ peak located at a binding energy of 856.23 eV with two satellite peaks located at binding energies of 862.12 eV and 878.87 eV can be assigned to NiO and $Ni(OH)_2$ [38]. This result is consistent with the EDS results that palladium, nickel, carbon, and oxygen are detected in the Pd-AC@NiO sample, while only nickel and oxygen are detected in the NiO sample.

Furthermore, XRD patterns have been recorded to identify the crystal structure of the as-prepared samples and shown in Fig. 4. Diffraction peaks at 37.3°, 43.3°, 63°, 75.4°, and 79.5° are perceived for the pure NiO. These peaks have been identified as peaks of cubic NiO crystallites with various diffracting planes (111), (200), (220), (311), and (222). This XRD pattern reveals the formation of the cubic phase of NiO (JCPDS Card No. 78–0429) with space group Fm3m and lattice constant, $a = 4.177$ Å. All the diffraction peaks are assigned to the NiO; no other diffraction peaks were detected in the XRD pattern of pure NiO, confirming that the metal oxide was free of impurities. While for the Pd-AC@NiO nanocomposite, the diffraction peaks at the Bragg angles of 40.3°, 46.85°, 68.4°, 82.4°, and 86.7° are observed, which are indexed to the (111), (200), (220), (311), and (222) diffracting planes of the cubic crystallite Pd. It has a broad peak around 23.8°, which can be ascribed to the (002) plane of the amorphous carbon structure. The other peaks observed at the Bragg angles of 44.5°, 51.9°, and 76.4° have been assigned to the (111), (200), and (220) diffracting planes of the Ni, respectively. It is important to note that three diffraction peaks of Ni are observed after decorating the Pd-AC over NiO, indicating the formation of metallic Ni. However, the intensity of Ni diffraction peaks is decreased significantly due to the decrease in Ni content in the Pd-AC@NiO nanocomposite, suggesting poor crystallinity as compared to the pure NiO. The Scherrer's formula was used to estimate the crystallite size based on the Pd (111) diffraction:

$$D = \frac{k\,\lambda}{\beta\,cos},$$

where D is the crystallite size (nm), K is the Scherrer constant (0.9), β is the corresponding full width at half maxima (FWHM, in radians), λ is the wavelength of X-ray (1.54 Å), and is the Bragg's diffraction angle. The calculated average

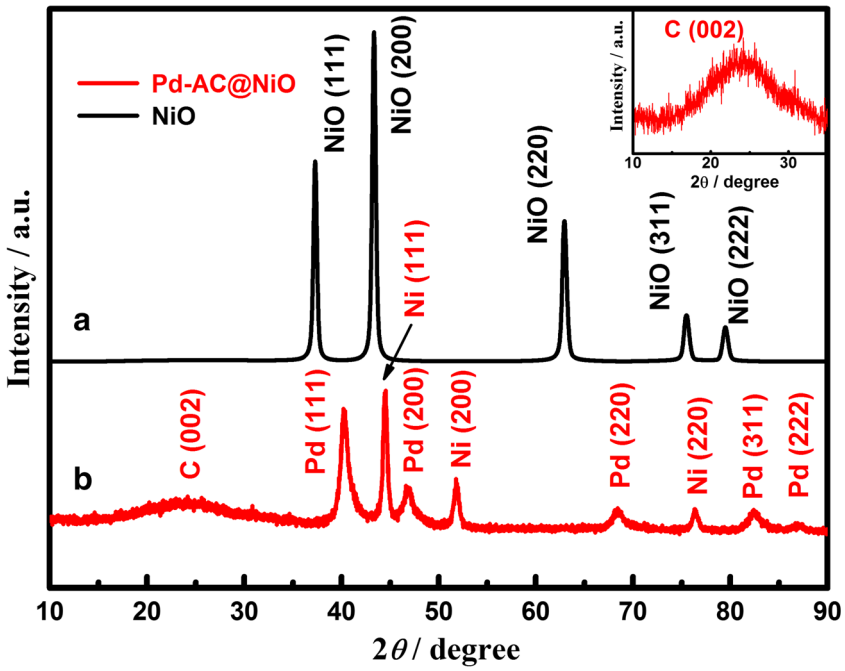

Fig. 4 XRD patterns of (**a**) NiO and (**b**) Pd-AC@NiO nanocomposite

crystallite particle size based on Pd (111) is found to be 10.31 nm for Pd-AC@NiO nanocomposite.

Remarkably, the pore size distribution and specific surface area of the electrode material plays an important role in the energy storage systems. Nitrogen adsorption-desorption isotherm measurements of the as-prepared NiO and Pd-AC@NiO nanocomposite are carried out at 77 K to characterize the structural characteristics and specific surface area. Nitrogen adsorption-desorption isotherm of NiO and Pd-AC@NiO samples are shown in Fig. 5 with their corresponding Barrette-Joyner-Halenda (BJH) pore size distribution. The N_2 adsorption-desorption isotherms for both Pd-AC@NiO and NiO samples display Type IV isotherm characteristics with a hysteresis loop (Fig. 5a and b) in the relative pressure (P/P_0) range of 0.02–0.99. Impressively, the BET specific surface area of Pd-AC@NiO nanocomposite(Fig. 5a) is 517.16m^2/g, which is much higher than that of the NiO (Fig. 5b) nanoparticles (297 m^2/g).

Moreover, Fig. 5c and d provides the pore size distributions for both Pd-AC@NiO and NiO samples, respectively, which is derived from the desorption isotherm. The BJH pore size distribution curve of the as-prepared NiO and Pd-AC@NiO samples is relatively broad, with a pore size distribution range of 3–11 nm, revealing that the as-prepared samples mainly contain mesopores. BJH calculations reveal that the average pore sizes of NiO and Pd-AC@NiO samples are 6.58 nm and 8.02 nm, respectively. Additionally, the pore volume of the Pd-AC@NiO sample is 0.133 cm^3/g, which is higher than that of NiO (0.084 cm^3/g). Furthermore, the large specific surface area, total pore volume, and improved pore size of the Pd-AC@NiO nanocomposite will provide sufficient reaction sites for ions and enhance the intercalation of electrolytic ions into the electrode during the electrochemical performance, which are more beneficial for improving the electrochemical performance.

Electrochemical analysis of the NiO nanoparticles and Pd-AC@NiO nanocomposite

Figure 6 demonstrates the electrochemical performance of the NiO and hybrid ternary nanocomposite (Pd-AC@NiO) as an electrode material for supercapacitors. To evaluate the electrochemical capacitive performance of the NiO and Pd-AC@NiO electrodes, cyclic voltammetry (CV) measurements were performed by using a three-electrode system in 2 M KOH aqueous electrolyte solution at different scan rates. The typical CV curves are achieved in the potential window of −1.8 V to 0.2 V for both the electrodes. Fig. 6a displays the CV curves of the hybrid ternary nanocomposite (Pd-AC@NiO) at different scan rates ranging from 10 to 50 mV/s. For attaining an obvious comparison, the capacitive performance of the supercapacitor electrode made from NiO nanoparticles is also measured in 2 M KOH aqueous electrolyte solution using a three-electrode system and their CV curves at different scan rates ranging from 10 to 50 mV/s are displayed in Fig. 6b. It can be seen in Fig. 6b that the CV curves of NiO electrode at different scan rates exhibit strong redox peaks, indicating a typical pseudocapacitive behavior and Faradaic reactions. When NiO nanoparticles are coupled with the Pd-AC material, the shape of the CV curves remains the same as the former, clearly shown in Fig. 6a. Besides, the redox peak position is changed with the increase of scan rate, but the

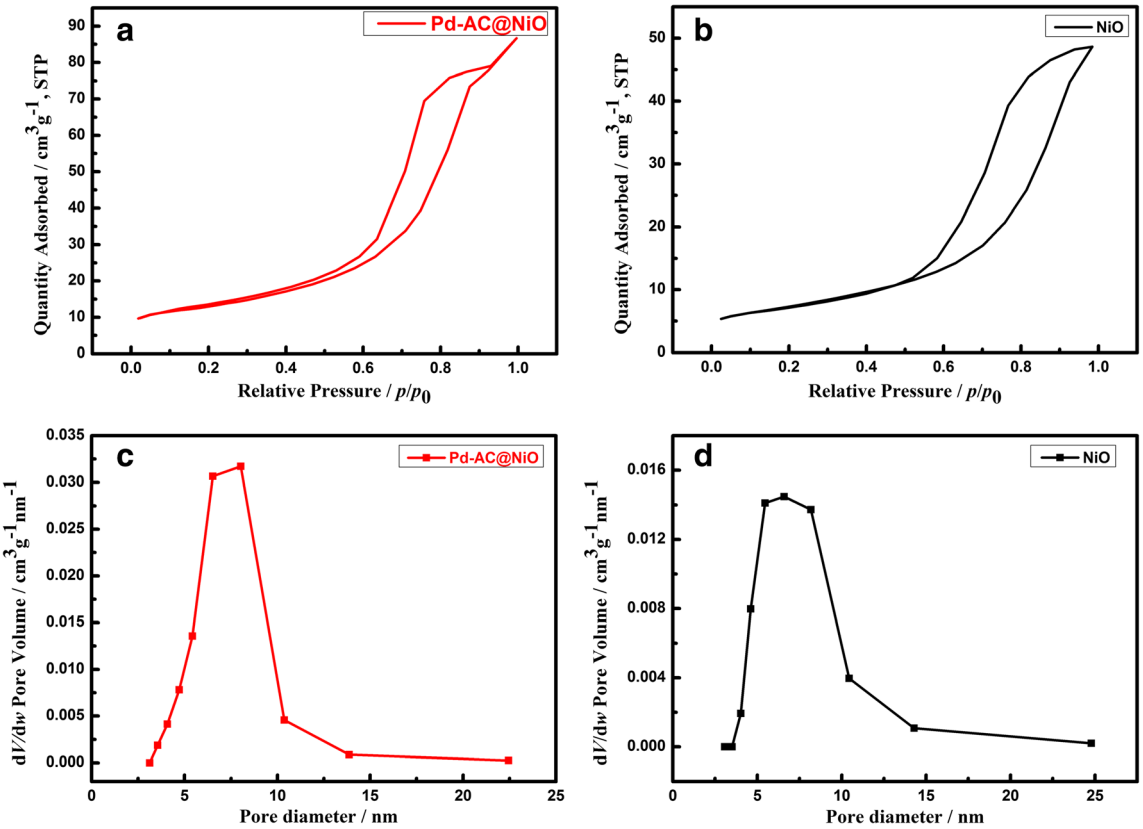

Fig. 5 Nitrogen adsorption-desorption isotherms of (**a**) Pd-AC@NiO nanocomposite, (**b**) NiO, and pore size distribution of (**c**) Pd-AC@NiO nanocomposite, (**d**) NiO

shape of the CV curves follows the same trend, illustrating the excellent rate performance and capacitive property for the practical applications. The specific capacitances of Pd-AC@NiO and NiO electrodes at different scan rates are calculated from their corresponding CV curves. The calculated specific capacitance for the same is plotted in Fig. 6c. The specific capacitance of the Pd-AC@NiO electrode is 1563.8, 1455.42, 1320.7, 1210.2, and 1056.5 F/g at scan rates of 10, 20, 30, 40, and 50 mV/s, respectively. In addition, the maximum specific capacitance for the Pd-AC@NiO electrode is 1563.8 F/g at a scan rate of 10 mV/s, which is much higher than that of NiO-based electrode (1239 F/g), displaying the successful incorporation of NiO nanoparticles into the composite structure. When the scan rate is increased from 10 to 50 mV/s, the specific capacitance (capacitance retention rate) of Pd-AC@NiO electrode and NiO electrode-based supercapacitors is decreased gradually from 1563.8 to 1056.5 F/g (67.5%) and 1239 to 801.6 F/g (64.6%), respectively. More importantly, it can be seen that at the same scan rate, the Pd-AC@NiO electrode performs better than the NiO electrode. Furthermore, the galvanostatic charging-discharging tests are performed in the applied potential difference window of 0–0.4 V at various current densities, ranging from 5 to 25 A/g, to evaluate the performance of the NiO, and Pd-AC@NiO electrode-based supercapacitors and their typical GCD curves are displayed in Fig. 6d and e respectively. As shown in Fig. 6d-e, the GCD curves for both the electrodes exhibit a nearly isosceles triangular shape with good symmetry at various current densities, suggesting the good charge propagation across the electrode. The specific capacitance of the samples obtained from the charge-discharge curves is shown in Fig. 6f at various current densities. From Fig. 6f, it can be seen that the Pd-AC@NiO electrode exhibits the specific capacitances of 1539, 1401.6, 1284.3, 1107.6, and1037.5 F/g at current densities of 5, 10, 15, 20, and 25 A/g, respectively. The Pd-AC@NiO electrode gives a high specific capacitance of 1539 F/g at a current density of 5 A/g, which is higher than that of the NiO electrode (1190 F/g at 5 A/g). This result validates that the Pd-AC@NiO nanocomposite combines the merits of pure metal oxide, metal, and carbon nanostructures.Concerning the specific capacitance and excellent rate performance, the Pd-AC@NiO nanocomposite shows superior performance than NiO nanoparticles for supercapacitors. This superior electrochemical performance is attributed due to the large specific surface area and porous structure. In this structure, mesopores facilitate fast ion diffusion, which leads to better rate performance.

To further investigate the energy density and power density of the supercapacitors based on NiO and Pd-AC@NiO electrodes, a Ragone plot is developed and is shown in Fig. 7a,

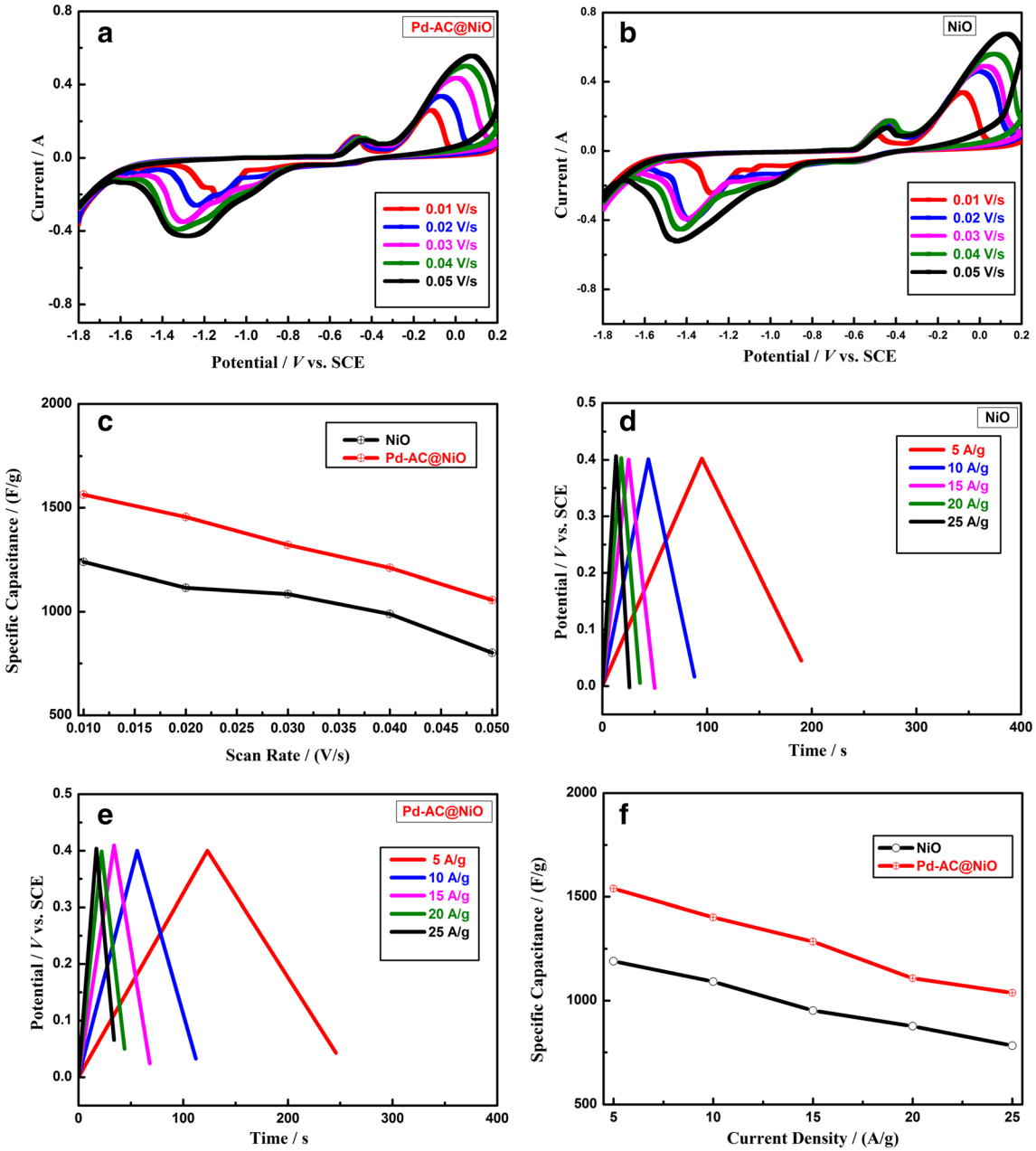

Fig. 6 Electrochemical characteristics in the three-electrode system. **a** CV curves of Pd-AC@NiO nanocomposite at different scan rates. **b** CV curves of NiO at different scan rates. **c** Calculated specific capacitance at different scan rates from CV curves. **d** GCD curve of NiO at different current densities. **e** GCD curves of Pd-AC@NiO nanocomposite at different current densities. **f** Calculated specific capacitance as a function of current densities from GCD curves

which involves the power densities and the corresponding energy densities at different current densities. As can be seen in the Ragone plots in Fig. 7a, the Pd-AC@NiO electrode-based device delivers a maximum energy density of 34.19 Wh/kg at the power density of 1000 W/kg, which is much higher than that of the NiO electrode-based device (26.4 Wh/kg at 1000 W/kg), whereas the energy densities for the Pd-AC@NiO and NiO based devices are still retained at the high values of 23.05 Wh/kg and 17.37 Wh/kg respectively, at a high power density of 4999 W/kg. From these results, it is notable that both of the devices have high energy density and high power density, especially the Pd-AC@NiO based device. In practical applications, the long term cycling stability is one of the most important parameters for supercapacitors. Therefore, stability tests are carried out to evaluate the stability of the composite electrode. The cycling stability of the NiO and Pd-AC@NiO based electrode was evaluated by the galvanostatic charge-discharge test at a constant charge-discharge current density of 15 A/g for 5000 cycles in a standard three-electrode system (Fig. 7b). The

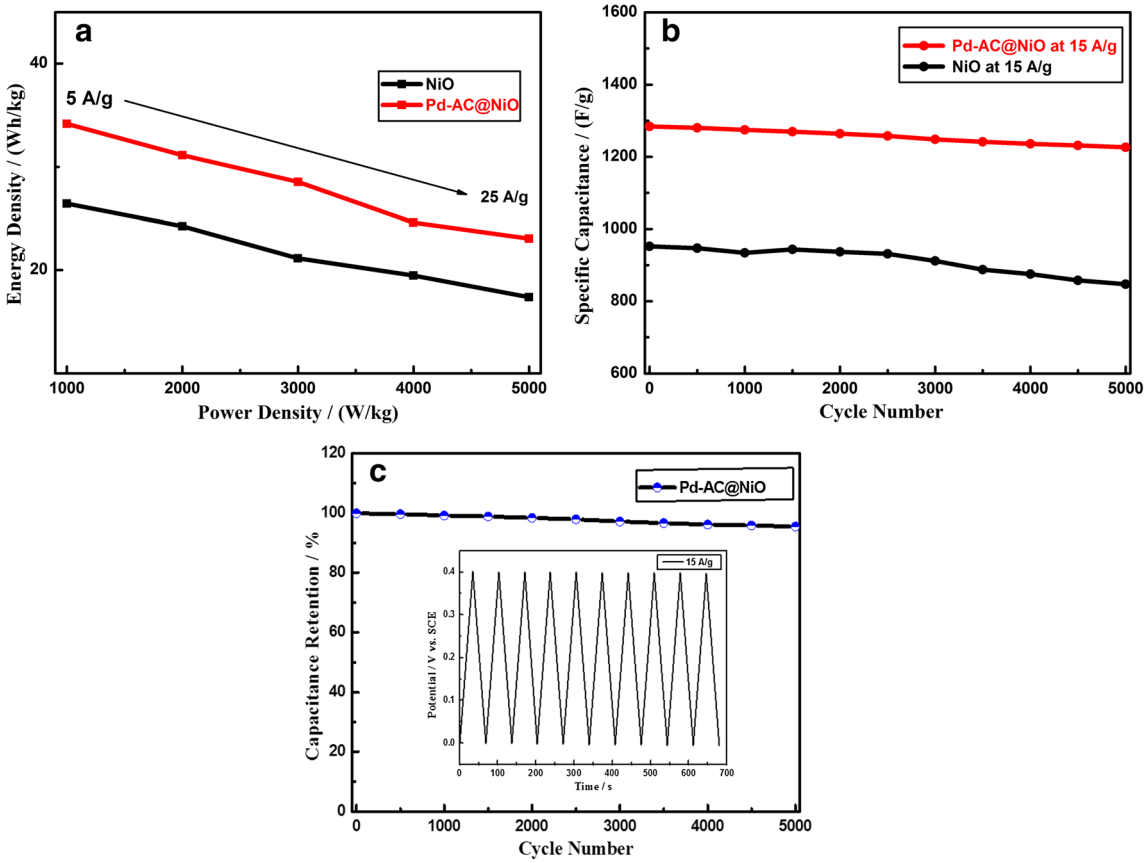

Fig. 7 **a** Ragone plots of NiO and Pd-AC@NiO nanocomposite, indicating the relationship between energy density and power density. **b** Cycling performance of NiO and Pd-AC@NiO nanocomposite at a current density of 15 A/g for 5000 cycles. **c** Capacitance retention of Pd-AC@NiO nanocomposite at a current density of 15 A/g for 5000 cycles (inset shows the cyclic performance for ten cycles)

specific capacitance of NiO and Pd-AC@NiO based electrode is 952.16 F/g and 1284.3 F/g, respectively at a current density of 15 A/g for the initial cycle and it still maintains a specific capacitance of 847 F/g and 1227 F/g after 5000 cycles for the same (Fig. 7b). As shown in Fig. 7c, the Pd-AC@NiO based electrode displays high capacitance retention of ~95.5% at 15 A/g for 5000 cycles (inset shows the corresponding GCD curve for ten cycles), endorsing its excellent cyclic stability and good cycle life.

During the testing process, it is found that specific capacitance decreased gradually with the increase in the cycle number. This is because when the cycle number is continuously increasing during the cycling stability test, the active material is gradually detached from the working electrode, which contributes to the lower specific capacitance. Overall, based on the numerous electrochemical tests, it is found that the hybrid ternary nanocomposite comprised of NiO, activated carbon, and Pd metal can significantly increase the specific capacitance and energy density as compared to pure metal oxide (NiO). Therefore, these results indicate that the Pd-AC@NiO nanocomposite is a very promising electrode material for supercapacitor applications.

Conclusions

In conclusion, a hybrid ternary nanocomposite comprised of NiO, AC, and Pd have been successfully fabricated by the co-precipitation method and are demonstrated as an electrode material and charge collector for high-performance electrochemical supercapacitors. In such a composite electrode, NiO provides the electroactive sites, which are favorable for storing the charge and energy, giving rise to a high specific capacitance. However, the introduction of Pd with AC onto the NiO surface not only improves the specific capacitance but also enhances the surface wettability of the electrode. Power density and rate capability of the composite electrode is significantly improved due to the high specific surface area of the carbon nanostructure. The synthesized Pd-AC@NiO hybrid ternary nanocomposite possesses an extremely high specific surface area of 517.16 m^2/g containing mesopores and micropores. Moreover, the fabricated hybrid ternary nanocomposite electrode material based on the Pd, AC, and NiO offer a specific capacitance of 1539 F/g at a charge-discharge current density of 5 A/g in 2 M KOH solution. The electrochemical performance of NiO nanoparticles reveals that the obtained

specific capacitance (1190 F/g at a charge-discharge current density of 5 A/g in 2 M KOH solution) is much lower than that of the hybrid ternary nanocomposite (Pd-AC@NiO) based supercapacitors. Benefiting to the high specific capacitance, the hybrid ternary nanocomposite electrode possesses a high energy density of 34.19 Wh/kg at a power density of 1000 W/kg. It also demonstrated excellent cycle stability with 95.5% specific capacitance retention after 5000 cycles. Therefore, the fabricated Pd-AC@NiO electrode shows good electrochemical performance concerning high specific capacitance, high energy and power density, excellent rate capability, and long cycling life, more competitive than those obtained by the NiO nanoparticles as an electrode material for supercapacitor. This result may be ascribed due to the fascinating properties of the composite material, such as high specific surface area, continuous electron transport path, and excellent wettability towards the electrolyte. Hence, our outcome proposes that this kind of hybrid ternary nanocomposite electrode can be a highly promising candidate for exploiting high-performance energy storage systems.

Acknowledgments S.S. acknowledges the fellowship support from the University Grant Commission (UGC) India. The authors are thankful to the CRF and NRF facilities provided by IIT Delhi.

Compliance with ethical standards

Conflict of interest The authors declare that there is no conflict of interest.

References

1. Gur TM (2018) Review of electrical energy storage technologies, materials and systems: challenges and prospects for large-scale grid storage. Energy Environ Sci 11(10):2696–2767
2. Aneke M, Wang M (2016) Energy storage technologies and real life applications- a state of the art review. Appl Energy 179:350–377
3. Mahlia TMI, Saktisahdan TJ, Jannifar A, Hasan MH, Matseelar HSC (2014) A review of available methods and development on energy storage: technology update. Renew Sust Energ Rev 33:532–545
4. Yang Z-R, Wang S-Q, Wang J, Zhou A-J, Xu C-W (2017) Pd supported on carbon containing nickel, nitrogen and sulfur for ethanol electrooxidation. Sci Rep 7(1):15479
5. Libich J, Maca J, Vondrak J, Cech O, Sedlarikova M (2018) Supercapacitors: properties and applications. Journal of Energy Storage 17:224–227
6. Muzaffar A, Ahamed MB, Deshmukh K, Thirumalai J (2019) A review on recent advances in hybrid supercapacitors: design, fabrication and applications. Renew Sust Energ Rev 101:123–145
7. Iro ZS, Subramani C, Dash SS (2016) A brief review on electrode materials for supercapacitors. Int J Electrochem Sci 11:10628–10643
8. Raza W, Ali F, Raza N, Luo Y, Kim K-H, Yang J, Kumar S, Mehmood A, Kwon EE (2018) Recent advancements in supercapacitors technology. Nano Energy 52:441–473
9. Miller EE, Hua Y, Tezel FH (2018) Materials for energy storage: review of electrode materials and methods of increasing capacitance for supercapacitors. Journal of Energy Storage 20:30–40
10. Hao P, Zhao Z, Li L, Tuan C-C, Li H, Sang Y, Jiang H, Wong CP, Liu H (2015) The hybrid nanostructure of $MnCo_2O_{4.5}$nanoneedle/carbon aerogel for symmetric supercapacitors with high energy density. Nanoscale 7(34):14401–14412
11. Vadiyar MM, Bhise SC, Patil SK, Kolekar SS, Shelke AR, Deshpande NG, Chang J-Y, Ghule KS, Ghule AV (2016) Contact angle measurements: a preliminary diagnostic tool for evaluating the performance of $ZnFe_2O_4$nano-flake based supercapacitors. Chem Commun 52(12):2557–2560
12. Fan Z, Yan J, Wei T, Zhi L, Ning G, Li T, Wei F (2011) Asymmetric supercapacitors based on grapheme/MnO_2 and activated carbon nanofiber electrodes with high power and energy density. Adv Funct Mater 21(12):2366–2375
13. Shi Q, Cha Y, Song Y, Lee J-I, Zhu C, Li X, Song M-K, Du D, Lin Y (2016) 3D graphene-based hybrid materials: synthesis and applications in energy storage and conversion. Nanoscale 8(34):15414–15447
14. Zhen L, Fan B, Junjie W, Weiwei Y, Liang W, Zhiwen C, Dengyu P, Minghong W (2018) Boosting the energy storage densities of supercapacitors by incorporating N-doped grapheme quantum dots into cubic porous carbon. Nanoscale 10:22871–22883
15. Padmanathan N, Selladurai S, Razeeb KM (2015) Ultra-fast rate capability of a symmetric supercapacitor with a hierarchical Co_3O_4 nanowire/nanoflower hybrid structure in non-aqueous electrolyte. RSC Adv 5(17):12700–12709
16. Shaikh JS, Pawar RC, Devan RS, Ma YR, Salvi PP, Kolekar SS, Patil PS (2011) Synthesis and characterization of Ru doped CuO thin films for supercapacitor based on bronsted acidic ionic liquid. Electrochim Acta 56(5):2127–2134
17. Hodaei A, Dezfuli AS, Naderi HR (2018) A high-performance supercapacitor based on N-doped TiO_2 nanoparticles. J Mater Sci Mater Electron 29:14596–14604
18. Xia X, Zhang Y, Chao D, Guan C, Zhang Y, Li L, Ge X, Bacho IM, Tu J, Fan HJ (2014) Solution synthesis of metal oxides for electrochemical energy storage applications. Nanoscale 6(10):5008–5048
19. Cao F, Pan GX, Xia XH, Tang PS, Chen HF (2014) Synthesis of hierarchical porous NiO nanotube arrays for supercapacitor application. J Power Sources 264:161–167
20. Yu W, Jiang X, Ding S, Li BQ (2014) Preparation and electrochemical characteristics of porous hollow spheres of NiO nanosheet as electrodes of supercapacitors. J Power Sources 256:440–448
21. Yuan G, Liu Y, Yue M, Li H, Liu E, Huang Y, Kong D (2014) Cu-doped NiO for aqueous asymmetric electrochemical capacitors. Ceram Int 40(7):9101–9105
22. Nagamuthu S, Ryu K-S (2019) Synthesis of Ag/NiO honeycomb structured nanoarrays as the electrode material for high-performance asymmetric supercapacitor devices. Sci Rep 9(1):4864
23. Chen J, Peng X, Song L, Zhang L, Liu X, Luo J (2018) Facile synthesis of Al-doped NiOnanosheet arrays for high-performance supercapacitors. R Soc Open Sci 5(11):180842
24. Wang Y, Su Q (2016) Synthesis of NiO/Ag nanocomposites by micro-emulsion method and the capacitance performance as electrodes. J Mater Sci Mater Electron 27:4752–4759
25. Vijayakumar S, Nagamuthu S, Muralidharan G (2013) Porous NiO/C nanocomposites as electrode material for electrochemical supercapacitors. ACS Sustain Chem Eng 9:1110–1118
26. Chen W, Gui D, Liu J (2016) Nickel oxide/graphene aerogel nanocomposite as a supercapacitor electrode material with extremely wide working potential window. Electrochim Acta 222:1424–1429
27. Yan Y, Wang T, Li X, Pang H, Xue H (2017) Noble metal-based materials in high-performance supercapacitors. Inorg.Chem.Front. 4(1):33–51

28. Wu JB, Li ZG, Lin Y (2011) Porous NiO/Ag composite film for electrochemical capacitor application. Electrochim Acta 56(5): 2116–2121
29. Qu B, Hu L, Chen Y, Li C, Li Q, Wang Y, Wei W, Chen L, Wang T (2013) Rational design of Au-NiO hierarchical structures with enhanced rate performance for supercapacitors. J Mater Chem A 1(24):7023–7026
30. Kalambate PK, Rawool CR, Karna SP, Srivastava AK (2018) Nitrogen-doped grapheme/palladium nanoparticles/porous poluaniline ternary composite as an efficient electrode material for high performance supercapacitor. Materials Science for Energy Technologies 2:246–257
31. Jiang W, Zhang K, Wei L, Yu D, Wei J, Chen Y (2013) Hybrid ternary rice paper-manganese oxide-carbon nanotube nanocomposites for flexible supercapacitors. Nanoscale 5(22):11108–11117
32. Mingjia Z, Chengcheng X, Jiangtian L, Ming L, Nianqiang W (2013) Nanostructured carbon-metal oxide composite electrodes for supercapacitors: a review. Nanoscale 5:72–88
33. Bose S, Kuila T, Mishra AK, Rajasekar R, Kim NH, Lee JH (2012) Carbon-based nanostructured materials and their composites as supercapacitors electrodes. J Mater Chem 22(3):767–784
34. Chen W, He Y, Li X, Zhou J, Zhang Z, Zhao C, Gong C, Li S, Pan X, Xie E (2013) Facilitated charge transport in ternary interconnected electrodes for flexible supercapacitors with excellent power characteristics. Nanoscale 5(23):11733–11741
35. Sk MM, Yue CY, Ghosh K, Jena RK (2016) Review on advances in porous nanostructured nickel oxides and their composite electrodes for high-performance supercapacitors. J Power Sources 308:121–140
36. Winkler K, Grodzka E, D'Souza F, Balch AL (2007) Two-component films of fullerene and palladium as materials for electrochemical capacitors. J Electrochem Soc 154(4):K1–K10
37. Dar RA, Giri L, Karna SP, Srivastava AK (2016) Performance of palladium nanoparticle-graphene composite as an efficient electrode material for electrochemical double layer capacitors. Electrochim Acta 196:547–557
38. Jin Y, Zhao J, Li F, Jia W, Liang D, Chen H, Li R, Hu J, Ni J, Wu T, Zhong D (2016) Nitrogen-doped graphene supported palladium-nickel nanoparticles with enhanced catalytic performance for formic acid oxidation. Electrochim Acta 220:83–90
39. Dhanushkotti R, Pulidindi IN, Arumugam P, Chinnathambi M (2018) Pd-NiO decorated multiwalled carbon nanotubes supported on reduced graphene oxide as an efficient electrocatalyst for ethanol oxidation in alkaline medium. Appl Surf Sci 442:787–796
40. Wang H-Q, Fan X-P, Zhang X-H, Huang Y-G, Wu Q, Pan Q-C, Li Q-Y (2017) In situ growth of NiO nanoparticles on carbon paper as a cathode for rechargeable Li-O_2 batteries. RSC Adv 7(38):23328–23333